Pharmaceutical Research, Vol. 27, No. 3, March 2010 (© 2009)
DOI: 10.1007/s11095-009-0035-8

Research Paper

Neuropilin-1 Targeting Photosensitization-Induced Early Stages of Thrombosis *via* Tissue Factor Release

Denise Bechet,[1] Loraine Tirand,[1] Béatrice Faivre,[2,3] François Plénat,[2,4] Corinne Bonnet,[4] Thierry Bastogne,[1,6] Céline Frochot,[5,6] François Guillemin,[1,6] and Muriel Barberi-Heyob[1,6,7]

Received September 16 2009; accepted December 9 2009; published online January 20, 2010

Purpose. This article characterizes the vascular effects following vascular-targeted photodynamic therapy with a photosensitizer which actively targets endothelial cells.
Methods. This strategy was considered by coupling a chlorin to a heptapeptide targeting neuropilin-1 in human malignant glioma-bearing *nude* mice. A laser Doppler microvascular perfusion monitor was used to monitor microvascular blood perfusion in tumor tissue. Endothelial cells' ultra structural integrity was observed by transmission electron microscopy. The consequences of photosensitization on tumor vessels, tissue factor expression, fibrinogen consumption, and thrombogenic effects were studied by immunohistochemical staining.
Results. Treatment of glioma-bearing mice with the conjugate showed a statistically significant tumor growth delay. Vascular effect was characterized by a decrease in tumor tissue blood flow at about 50% baseline during treatment not related to variations in temperature. This vascular shutdown was mediated by tumor blood vessels' congestion. A pro-thrombotic behavior of targeted endothelial cells in the absence of ultra structural changes led to the induction of tissue factor expression from the earliest times post-treatment. Expression of tissue factor-initiated *thrombi* formation was also related to an increase in fibrinogen consumption.
Conclusion. Using a peptide-conjugated photosensitizer targeting neuropilin-1, induction of tissue factor expression immediately post-treatment, led to the establishment of thrombogenic effects within the vessel *lumen*.

KEY WORDS: blood flow; endothelial cells; neuropilin-1; thrombogenic effect; tissue factor.

Loraine Tirand and Béatrice Faivre contributed equally to this study.

[1] Centre de Recherche en Automatique de Nancy (CRAN), Nancy-University, CNRS, Centre Alexis Vautrin, Avenue de Bourgogne, Brabois, 54511, Vandœuvre-lès-Nancy, France.
[2] EA 4421 SiGReTO, Faculté de Médecine, Vandœuvre-lès-Nancy, France.
[3] Laboratoire d'Hématologie, Faculté de Pharmacie, Nancy-University, Nancy, France.
[4] Laboratoire d'Histopathologie Expérimentale et Moléculaire, Faculté de Médecine, Nancy-University, Nancy, France.
[5] Département de Chimie Physique des Réactions (DCPR), Nancy-University, CNRS, Nancy, France.
[6] GDR CNRS 3049 "Médicaments Photoactivables-Photochimiothérapie (PHOTOMED)", Vandœuvre-lès-Nancy, France.
[7] To whom correspondence should be addressed. (e-mail: m.barberi@nancy.fnclcc.fr)

ABBREVIATIONS: Ahx, 6-aminohexanoic acid; a.i., arbitrary intensity; ATWLPPR, H-Ala-Thr-Trp-Leu-Pro-Pro-Arg-OH; asHTF, alternatively spiced human tissue factor; a.u., arbitrary units; BPD-MA, benzoporphyrin derivative monoacid ring; BSA, bovine serum albumine; DLI, drug-light interval; FITC, fluoresceine iso thio cyanate; HES, hematoxylin, eosin and safran; HRP, streptavidin-horseradish peroxidase; IL-6, interleukin-6; i.v., intravenous; NRP-1, neuropilin-1; PBS, phosphate-buffered saline; PDT, photodynamic therapy; PEG, polyethylene glycol; PO_2, oxygen pressure; ROS, reactive oxygen species; RSM, response surface methodology; s.d., standard deviation; TEM, transmission electron microscopy; TEM buffer, Tris EDTA molybdate buffer; TF, tissue factor; TGD, tumor growth delay; TNF-α, tumor necrosis factor alpha; TPC, 5-(4-carboxyphenyl)-10,15,20-triphenylchlorin; V, volume; VEGF, vascular endothelial growth factor; VTP, vascular targeted photodynamic therapy.

INTRODUCTION

Photodynamic therapy (PDT) uses a photo-active compound, light, and oxygen to create tissue damage. Three mechanisms by which PDT destroys tumors include (1) direct tumor cell kill, resulting from lethal events initiated by the flux of reactive oxygen species (ROS); (2) post-treatment inflammatory and immune responses directed against the tumor cells; and (3) damage to the tumor-associated vasculature. Destruction of the vasculature may indirectly lead to tumor eradication, following deprivation of life-sustaining nutrients and oxygen (1,2), and this vascular effect is thought to play a major part in the destruction of some vascularized tumors by PDT (3–9). Hence, tumor vasculature is a potential target of PDT damage. The preference of vascular targeting is highly dependent upon the relative distribution of photosensitizers in each compartment, which is related to their pharmacokinetic properties and can be favored by choosing short drug-light intervals (DLI), or by modifying the photosensitizer molecular structure. This passive targeting mechanism is regulated by the photosensitizer physicochemical properties. Indeed, photodynamic treatment using shorter DLI mainly targets tumor vasculature, and loss of vascular barrier function has been observed shortly following vascular-targeting PDT (10,11). This first strategy has been selected by Kurohane *et al.*: laser irradiation 15 min after injection of the liposomal benzoporphyrin derivative monoacid ring BPD-

MA caused haemostasis due to damage to angiogenic endothelial cells. This approach suppressed tumor growth more efficiently than conventional PDT (12). Only a very limited number of studies have been performed to actively target tumor vascular endothelial cells (13). Receptors specifically located on angiogenic endothelial cells, such as receptors to vascular endothelial growth factor (VEGF), can be used as molecular targets. We have previously described the conjugation of a photosensitizer (a chlorin) to an heptapeptide (ATWLPPR), specific for the VEGF receptor, neuropilin-1 (NRP-1) (14,15). We evidenced a significant decrease of the conjugated photosensitizer cellular uptake after RNA interference-mediated silencing of NRP-1 (16). This new targeted photosensitizer proved to be very efficient *in vitro* in human umbilical vein endothelial cells compared to its non-conjugated counterpart (15). *In vivo*, we also demonstrated the interest of using this active-targeting strategy, allowing efficient tumor tissue uptake of the conjugated photosensitizer. In mice xenografted ectopically with U87 human malignant glioma cells, we demonstrated that only the conjugated photosensitizer allowed a selective accumulation in endothelial cells lining tumor vessels (17). The time of 4 h post-injection corresponded, according to microscopy analyses, to highest incorporation of the conjugated photosensitizer in endothelial cells (before that time, *e.g.,* at 1 h post-injection, the conjugate was mostly localized in the plasma). Conversely, TPC showed only faint and diffuse staining in the tumor, with no specific localization in endothelial cells (17). This short DLI was also chosen corresponding to relevant conjugate levels in tumor and low degradation of the peptidic moiety. Using the response surface methodology (RSM), an optimal vascular-targeted photodynamic therapy (VTP) condition was selected to model effects and interactions of photosensitizer dose, fluence and fluence rate on the growth of U87 human malignant glioma cells ectopic xenografted in nude mice (18). In this study, photodynamic treatment of glioma-bearing mice using the peptide-conjugated photosensitizer validated the decrease in tumor growth compared to animals who received the treatment with the non-conjugated photosensitizer. Thus, we postulated that the improvement of tumor responsiveness with the conjugated photosensitizer originated from the procedure producing the anti-vascular effect. A mechanistic understanding of photosensitization-induced early thrombogenic events was necessary. This article characterizes the vascular effects following PDT with this novel photosensitizer and demonstrates that the induction of tissue factor (TF) expression following treatment leads to the establishment of tumor blood vessel congestion.

MATERIALS AND METHODS

Photosensitizer

We described previously the conjugation of a photosensitizer (5-(4-carboxyphenyl)-10,15,20-triphenylchlorin, TPC), *via* a spacer (6-aminohexanoic acid, Ahx), to an heptapeptide (H-Ala-Thr-Trp-Leu-Pro-Pro-Arg-OH, noted ATWLPPR). TPC was purchased from Frontier Scientific (Logan, UT). TPC-Ahx-ATWLPPR was synthesized and purified as described previously (15,19). Stock solutions in dimethylsulfoxide (2 mM) were used. The photosensitizers were diluted in polyethylene glycol (PEG) 400/ethanol/water (30:20:50, *v/v/v*) to the concentration required for intravenous (i.v) injection to mice (200 µL/25 g body weight). For each experiment, concentrations were checked with a Perkin-Elmer UV-visible spectrophotometer (Lambda 2, Courtaboeuf, France), using the molar extinction coefficients reported previously (15).

Animals and Tumor Model

Female athymic Foxn1 nude mice (*nu/nu*) were used for this study (Harlan, Gannat, France). Animal care and studies were performed according to the European convention for the protection of Vertebrate Animals Used for Experimental and Other Scientific Purposes, EU directives and The Law on Statute on Animal Experiments in France. Mice (6–7/cage) were maintained in standard cages in isolators. Animals were housed with 12-hour light/dark cycle at 22–24°C and 50% humidity, and they were administered with food and water *ad libitum*. The mice were used for tumor implantation when they were 7–9 weeks old (20–25 g). They were anesthetized using an intraperitoneal injection of a mixture of ketamine (Ketalar®, Panpharma, Fougères, France) and xylazine (Rompun®, Bayer Pharma, Puteaux, France) at a dose of 60 mg/kg and 8 mg/kg, respectively. The model of human malignant glioma was obtained using U87 cells (20). Tumors were treated when they reached a treatment size of 5±1 mm geometric mean diameter (15±5 days after tumor grafting, (16)).

PDT Efficiency *In Vivo*

In practice, the four factors that are usually considered for PDT treatment are the administered photosensitizer dose, DLI, light fluence and light fluence rate. To limit the number of experiments to be carried out, in our approach, a DLI of 4 h was selected. By fixing this parameter, the determination of the optimal PDT dosimetry was expressed as the optimal choice of the three remaining factors (photosensitizer dose, light fluence and fluence rate), *i.e.* selection of values leading to an optimal PDT response. A Doehlert experimental design was selected to model effects of photosensitizer dose, fluence and fluence rate on the growth of U87 human malignant glioma cells xenografted in nude mice. An optimal PDT condition was selected (photosensitizers dose : 2.80 mg/kg (1.75 µmol/kg); fluence : 120 J/cm^2; fluence rate : 85 mW/cm^2) (18). The dose for each photosensitizer was injected to the mice *via* the tail vein. The mice were kept in the dark for 4 h and anesthetized as described above. Irradiation of tumors was carried out at 652 nm, using a dye laser (SpectraPhysics 375B, Les Ulis, France) pumped with an argon laser (Spectra-Physics 2020). Light was delivered through an optical fiber (HCG type, SEDI Fibres Optiques, Courcouronnes, France) and a light distributor (Frontal Diffuser FDI, Medlight SA, Ecublens, Switzerland) for a perfectly homogeneous illumination of the spot, which illuminated the tumor surface over a 1-cm diameter beam spot. The incident fluence rate on the tumors was evaluated using an optical power meter (SP407, SpectraPhysics). At least six mice were used for each group. The control group consisted of mice that did not receive any treatment (no photosensitizer,

no light) (18). Following VTP, tumor diameter was measured three times a week in two orthogonal directions using an electronic caliper, and tumor volume (V) was calculated using the *formula*

$$V = \left(\text{length} \times \text{width}^2\right)/2$$

Measurements were carried out during 50 days or until tumors reached a size of 1 cm^3, at which time mice were sacrificed by cervical dislocation.

Measurements of Oxygen, Temperature and Microvascular Blood Flow

A 100 μm diameter thermocouple and two 230 μm fibers are attached to the probe. This combined probe measures oxygen, temperature, and microvascular blood flow. The measurement requires OxyLite and OxyFlo instruments. OxyLite 2000 (Oxford Optronix, Oxford, UK) is a two-channel device (measuring PO_2 and temperature at two sites simultaneously), and OxyFlo 2000 is a two-channel laser Doppler perfusion monitoring instrument. The OxyLite has been designed to operate in conjunction with the OxyFlo. The probe calibration parameters are transferred from the probe packaging to the OxyLite instrument using the bar code wand. For each PO_2 input on the OxyLite front panel, there is a corresponding temperature input. A thermocouple sensor may be attached to these temperature inputs using the thermocouple adapters provided. The OxyFlo is a laser Doppler flow meter whose primary purpose is to measure real-time microvascular red blood cell perfusion. Laser Doppler signals were recorded in blood perfusion unit, which is a relative unit scale, defined using a carefully controlled motility standard. The OxyFlo was calibrated before leaving the factory, using a motility standard solution of carefully selected latex spheres undergoing Brownian motion. A relative measure, the blood perfusion unit, was the output of the flow meter and is representative of local flow at the distal tip of the probes. Before the experiments, all probes were calibrated by way of the kit supplied by the manufacturer. The ongoing standardization also followed the manufacturer's procedures. A low light power (<0.5 mW) was applied by a laser diode integrated into the system. The wavelength of 830 nm enables it to follow front blood flow, during and after PDT. Measurements were representative of a volume of 0.3–0.5 mm^3 near the probe and were recorded 5 min before the beginning of treatment, during VTP and 5 min after treatment. When the mouse was sacrificed, the value of the residual flow obtained after stabilization of the signal was indicated "the physiological zero." This value was withdrawn from the whole of the measured values, and the results were presented in the form of percentage compared to the flow before irradiation.

Endothelial Cells Ultra Structural Integrity by Transmission Electron Microscopy

Just after treatment, tumors were fixed in 2.5% glutaraldehyde in 0.1 M phosphate buffer overnight at 4°C. Full thickness biopsies were cut into thin pieces and washed with 0.1 M sodium cacodylate buffer, pH 7.2, for 2 h. Subsequently, they were fixed in 1% osmium tetroxide solution for 20 min, washed in 0.1 M phosphate buffer (pH 7.2) for 90 min and washed once again with sodium cacodylate buffer. The samples were dehydrated through series of graded alcohol, embedded in resins Epon and sectioned into semithin-sections (2 μm), which were stained with toluidine blue. Ultrathin sections (75 nm) were sectioned from semithin sections, contrasted with uranyl acetate agent and lead citrate to improve contrast of cellular organelles. Ultrathin sections were observed using transmission electron microscopy (TEM; CM10, Philips, Eindhoven, The Netherlands). All chemicals were purchased from Sigma (Saint Quentin Fallavier, France), unless otherwise stated.

Co-expression of TF and Collagen IV by Immunohistochemical Staining

The tumor tissues were coated with Tissue-Tek® OCT (Sakura Firetek, Torrance, CA, USA) and placed first in liquid nitrogen-cooled isopentane for at least 40 s to completely freeze the biopsy and, afterwards, placed at −80°C. The sections (approximately 5–7 μm thick) were fixed with poly-(ethylene glycol) (PEG) for 10 min, hydrated in phosphate-buffered saline (PBS) with 0.05% Tween 20 (Dulbecco's PBS, Gibco, Invitrogen Corporation, Scotland), and incubated for 4 h at room temperature with the primary rabbit anti-mouse TF monoclonal antibody (extracellular domain of mouse tissue factor comprising amino acids 29–250) (1:320 in dilution buffer: PBS pH 7.4 with 0.1% (*m*/*v*) sodium azide, 0.06% (*m*/*v*) N-ethylmaleimide, 1% (*m*/*v*) BSA, 30% (*v*/*v*) glycerol; American Diagnostica Inc., Stamford, CT). After washing, the sections were incubated for 1 h with secondary goat anti-rabbit biotinylated polyclonal immunoglobulins (diluted 1:200 in PBS-Tween; Dakocytomation, Denmark). The revelation of secondary biotinylated antibodies was performed with a streptavidin-horseradish peroxidase complex (1 h at room temperature, diluted 1:200 in PBS-Tween;, Dakocytomation, Denmark) and the peroxidase substrate (5 min, Vector® NovoRed™ Substrate Kit for peroxydase, HistoGreen, Vector Laboratories, Paris, France).

To make the localization of TF expression precise, a collagen IV immunostaining was performed. The sections were incubated with 0.1 M HCl for 20 min, washed and incubated for one night at 4°C with the primary rabbit anti-mouse collagen IV monoclonal antibody (diluted 1:3000 in PBS;fs Novotec, Wittelsheim, France). After washing with PBS-Tween, the sections were incubated for 1 h at room temperature with the secondary goat anti-rabbit biotinylated polyclonal immunoglobulins (diluted 1:200; Clinisciences). The revelation of secondary biotinylated antibodies was performed as described above. Then, a hematoxylin counterstaining was performed to visualize the section by optical microscopy (AX-70 Provis, Olympus, Rungis, France).

Assessment of Fibrinogen Consumption by Immunofluorescence Staining

The tumor tissue was prepared as described above, using Tissue-Tek® OCT. The sections were air-dried and washed in isotonic PBS. To localize the vessels, the sections were incubated for 3 h with the primary rabbit anti-mouse collagen

IV monoclonal antibody (1:3200 dilution; Novotec) and for 1 h with the secondary goat anti-rabbit biotinylated polyclonal immunoglobulins. The secondary antibody was revealed using a Texas red streptavidin complex (1:4000 diluted in Tris-buffered saline Tween®20; Streptavidin Fluoprob, Interchim, Montluçon, France). To determine the consumption of fibrinogen, the sections were incubated with polyclonal rabbit anti-Human Fibrinogen/FITC (fluoresceine isothiocyanate) (1:20 dilution, Dakocytomation, Denmark) for 30 min. The co-distribution of collagen IV and fibrinogen was visualized by fluorescence microscopy (Axioskope 2, Zeiss) using an excitation filter (band-pass 455–495 nm or 540–552 nm, respectively) and emission filter (band-pass 505–555 nm or 565–595 nm), respectively.

Assessment of Intravascular Thrombosis by Histopathology, with Vascular Immunohistochemistry

To make the effects of VTP targeting angiogenic endothelial cells on tumor functional vasculature precise, tumor tissues were fixed during 24 h at room temperature in a buffer (0.1 M Tris-HCl, pH 7.4, 3.2 mM calcium acetate, 22.8 mM zinc acetate, 36.7 mM zinc chloride). Histopathology was performed on 5 μm paraffined tissue sections. For each condition tested (control, both photosensitizers, different times after treatment), a hematoxylin, eosin and safran (HES) staining was performed. To detect thrombogenic effect of PDT in the vessels, another adjacent section was incubated for 3 h at room temperature with the primary rat anti-mouse CD31 antibody (1:20 dilution buffer; Pharmingen/BD Biosciences, Le-Pont-de-Claix, France). After washing, the slides were incubated for 1 h with the secondary rabbit polyclonal anti-rat biotinylated IgG (1:400 dilution in PBS-Tween; Clinisciences). The revelation of secondary biotinylated antibodies was performed with a streptavidin-horseradish peroxidase complex (1 h at room temperature, diluted 1:400 in PBS-Tween, Dakocytomation, Denmark) and the peroxidase substrate (5 min, Vector® NovoRed™ Substrate Kit for peroxydase, HistoGreen, Vector Laboratories, Paris, France). Then, a hematoxylin counterstaining was performed to visualize the section by optical microscopy (AX-70 Provis, Olympus, Rungis, France).

Protein Extraction and Bio-Plex® Mouse Cytokine (TNF (tumor necrosis factor)-α and IL(interleukin)-6) Assays (21)

Proteins were extracted from tumor frozen specimens using Cell Lysis kit (Bio-Rad, Marnes La Coquette, France) according to the manufacturer's recommendations. Half of the tumor specimens were first disrupted using steel bead tissue lyser (Quiagen, Courtaboeuf, France) for 15 min. Disrupted tumor tissues were exposed to the lysis solution, scrapped, then transferred into microvial (Eppendorf®, Lepecq, France) and centrifuged at 4,500 *g* for 20 min at 4°C. Protein-containing supernatants were then collected and stored frozen at −80°C until analyzed. Before being analyzed, the protein concentration was determined in each extract using 690 nm colorimetric DC Protein assay kit (Bio-Rad) based on Lowry technique. The expression of the signaling cytokine was analyzed using Bioplex® cytokine assay (Bio-Rad) based on multiplex sandwich bead immunoassays. Protein extracts were transferred into 96-well dishes and diluted with 25 μl buffered solution. Fluorescent-capturing beads coupled to antibodies directed against TNF-α and IL-6 were mixed. The antibody-conjugated beads were added into each well and incubated 30 min. Following incubation, the plates were washed and incubated with biotinylated antibodies fixing each target protein. Streptavidin-phycoerythrin solution was then added. The analysis consisted of a double laser fluorescence detection allowing simultaneous identification of the target protein through the red fluorescence emission signal of the bead and quantification of the target phosphoprotein through the fluorescence intensity of phycoerythrin. Positive control, consisting of standard protein extract from control cell line was added to each series. Results were recorded as mean fluorescence intensities and normalized to the data measured in the positive controls.

Statistical Analysis

The Pearson correlation coefficient was used to study the linear dependence between mean fibrinogen and mean collagen staining. Efficacy of PDT according to the response surface methodology was presented with the Kaplan-Meier model, considering the percentage of tumors not having reached 10 times their initial volume as the end-point. Statistical analysis was conducted through the log-rank test. Mann-Whitney U test was used to assess the significant level between independent variables. The level of significance was set to $p<0.05$.

RESULTS

Mice treated by PDT with TPC-Ahx-ATWLPPR showed a statistically significant therapeutic efficacy, compared to the TPC-treated group (Fig. 1A). No significant difference was observed between the control group and the TPC-treated group. Control groups (*i.e.* light only, TPC only and TPC-Ahx-ATWLPPR only) were also used; no significant difference could be observed between these groups (data not shown). Tumor growth curves with the targeted photosensitizer resulted in stabilization of almost all tumor volumes within 10 days post-treatment (Fig. 1B). Nevertheless, interestingly, the mean diameter at day 2 for the group treated by TPC-Ahx-ATWLPPR was significantly higher than before PDT, also followed by a significant decrease at day 6 ($p=0.016$ and 0.040, respectively; Fig. 1D). Histologic examination of CD31 staining tissue sections, taken from tumors at 24 h after vascular-targeting PDT, indicated extensive vascular disruption, oedema tissue and mixed types of cell death, necrosis and apoptosis with condensed and/or fragmented nuclear morphology throughout tumor sections with both photosensitizers (Fig. 1C). Increased induction of cytokines TNF-α and IL-6 was observed a few minutes only after TPC-Ahx-ATWLPPR-induced VTP (Fig. 1E).

Laser Doppler technology offers the advantage of continuous blood-flow monitoring during PDT. Tumor blood flow was measured continuously before the start of treatment until 5 min after the conclusion of PDT (Fig. 2A). In TPC-Ahx-ATWLPPR-PDT-treated animals, a rapid increase in blood flow occurred during the first 3 min of treatment. Following this PDT-induced increase, blood flow decreased at about 50% of baseline, resulting in a characteristic biphasic

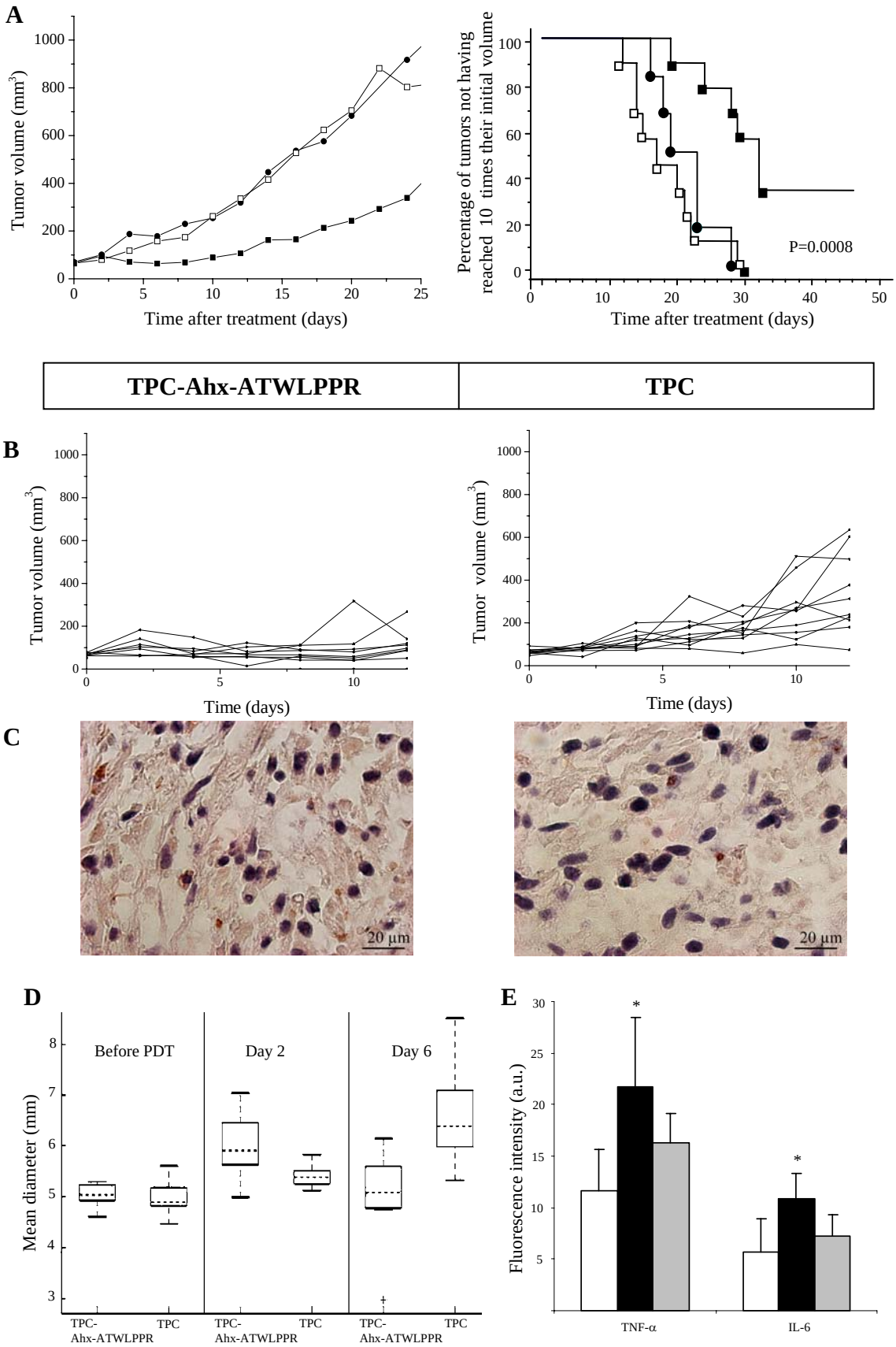
A
Tumor volume (mm3)
Time after treatment (days)
Percentage of tumors not having reached 10 times their initial volume
P=0.0008
Time after treatment (days)
TPC-Ahx-ATWLPPR
TPC
B
Tumor volume (mm3)
Time (days)
Tumor volume (mm3)
Time (days)
C
20 µm
20 µm
D
Mean diameter (mm)
Before PDT
Day 2
Day 6
TPC-Ahx-ATWLPPR
TPC
TPC-Ahx-ATWLPPR
TPC
TPC-Ahx-ATWLPPR
TPC
E
Fluorescence intensity (a.u.)
TNF-α
IL-6

Fig. 1. Vascular-targeted PDT induced tumor growth delay. *A*, using optimal treatment condition (fluence rate = 85 mW/cm^2, fluence = 120 J/cm^2, dose = 1.75 μmol/kg) deduced from RSM (18), tumor growth curves following treatment with TPC-Ahx-ATWLPPR [*black squares*] were compared to growth curves with TPC [*white squares*]. Light-only control group was represented [*black circles*]. **A** no significant difference could be observed between the control group and the TPC-treated group. On the contrary, mice treated by PDT with TPC-Ahx-ATWLPPR showed a tumor growth delay compared to the TPC-treated group (data points show the median tumor volume). Kaplan-Meier curves of control mice or mice treated by PDT, using TPC or TPC-Ahx-ATWLPPR considering the percentage of tumors not having reached 10 times their initial volume at the end point (*right*). At least nine mice were used for each experimental group. Statistical analysis was performed using the log-rank test (p values represent comparison TPC *versus* TPC-Ahx-ATWLPPR). **B** tumor growth curves following treatment for all animals during 10 days. **C** histological images of CD31 staining counterstained with hematoxylin obtained from tumor sections of the U87 tumors 24 h after PDT (same optimal conditions) using TPC-Ahx-ATWLPPR (*left*) or TPC (*right*). **D** boxplots of tumor mean diameters before treatment and at day 2 and 6 post-PDT. **E** increased expression of TNF-α and IL-6 in tumors, following treatment with TPC-Ahx-ATWLPPR [*black*] and TPC [*white*]. The induction of both cytokines was compared to control tumors (no-light). Data represent mean ± s.d.; $n=4$ samples per group, $*p<0.05$ *versus* control.

change in tumor blood flow (22,23). The first minimum was reached at about 10 min after the start of treatment, but the time to the trough varied widely among tumors. With TPC-mediated PDT as control, minor fluctuations in blood flow were detected during illumination. However, PDT may induce hyperthermia and thus also affect tumor blood flow. To evaluate thermal effect of our VTP protocol, we monitored tissue temperature during treatment with both photosensitizers (Fig. 2A). Whatever the photosensitizer, the tumor tissue temperature increased in a comparable manner, ranging between 1.6°C and 1.9°C during the photodynamic treatment. This increase would not be expected to affect the tumor vasculature. In a study by Dudar and colleagues, normal tissue from rabbits required temperatures greater than 47°C to bring about vascular stasis in less than 1 hour, while stasis occurred in tumors in the same time frame at temperature greater than 41°C (24). We measured no significant variation of tumor oxygenation before and immediately after VTP, no matter the photosensitizer (Fig. 2A).

To determine the cause of reduction in blood flow using the laser Doppler experiments, damage to vasculature in the periphery of the tumors (which often have both wide vessels and high vessel densities) was first evaluated histologically. Extensive platelet aggregation and red blood cell agglutination were observed into blood vessels of the tumor capsule from animals treated with TPC-Ahx-ATWLPPR as soon as treatment ended (Fig. 2B).

In order to elucidate the precise mechanism that was responsible for the coagulation initiation post-treatment, we studied the effects of TPC-Ahx-ATWLPPR photosensitization on endothelial cells morphology. Vessel walls were first identified as CD31-positive structures (Fig. 3A). A strong and distinct staining, predominantly membranous but also cytoplasmic, of vascular endothelial cells was observed with both photosensitizers. The staining was observed in the vascular endothelial cells of the wide and small vessels. We secondly showed that the ultra structural morphology of endothelial cells did not seem to be impaired as checked by TEM, no matter the photosensitizer (Fig. 3B).

Disturbance of endothelial cells through vascular injury could also result in an increase in expression of procoagulant mediators (25). As illustrated in Fig. 4B, the increased expression of TF is the major event during vascular dysfunction resulting in a highly thrombogenic environment (26). We examined if VTP targeting endothelial cells could affect TF expression. An intense TF expression was observed a few minutes only after TPC-Ahx-ATWLPPR-induced VTP (Fig. 4A). As control tumors using either light only or photosensitizers only, TPC-induced photodynamic activity induced no TF expression compared to the peptide-conjugated photosensitizer. Fibrinogen expression in tumor tissue was compared between TPC-mediated PDT and animals who received the conjugated photosensitizer. Moreover, to gain an insight into localization of fibrinogen in the tumor tissue, we undertook an immunohistochemical analysis of type IV collagen-staining (Fig. 4C). Immediately post-treatment, we calculated no colocalization for TPC, whereas tumors treated with TPC-Ahx-ATWLPR exhibited a marked colocalization between both staining. Four hours post-treatment, an increase of relative fibrinogen staining was evaluated for TPC; on the contrary, a decrease of fibrinogen expression was evidenced concerning the conjugate (Fig. 4C).

The thrombogenic effect after TPC-Ahx-ATWLPPR-induced VTP was confirmed by histological examination with blood stasis in all regions examined 2 h post-treatment (Fig. 5A), followed by *thrombi* in vessel lumen 4 h post-treatment (Fig. 5B).

DISCUSSION

The goal of tumor vascular targeting is to selectively modulate tumor vascular function in order to lead to a therapeutic purpose (27). To achieve this aim, therapeutic molecules need to be selectively delivered to the tumor vascular targets. A variety of tumor vascular molecular markers have been suggested for a selective targeting through conjugating therapeutic agents with tumor vasculature homing molecules; nevertheless, a marker that is absolutely specific for tumor vasculature has not yet been and may never be described (28). In PDT, a passive targeting of tumor vasculature might be practically the most effective approach to target tumor blood vessels. This passive targeting can be obtained either by changing PDT scheduling (*i.e.* by decreasing DLI), or by designing photosensitizers localizing primarily in the vascular compartment. The first method has been suggested by Kurohane *et al.* describing hemostasis due to damage to angiogenic endothelial cells (12). This approach suppressed tumor growth more efficiently than conventional PDT. This method has also been suggested with a novel photosensitizer MV6401, a pyropheophorbide derivative with indium chelated in the center of the pyropheophorbide macrocycle (29). The authors determined that PDT-induced vascular effects occurred rapidly with an acute response immediately after PDT and a-long-term response at times greater than 3 h after treatment. MV6401-mediated photodynamic treatment produced selective vascular effects, including vasoconstriction, vascular shutdown, *thrombi* formation and *in fine* tumor growth delay. The second method involves

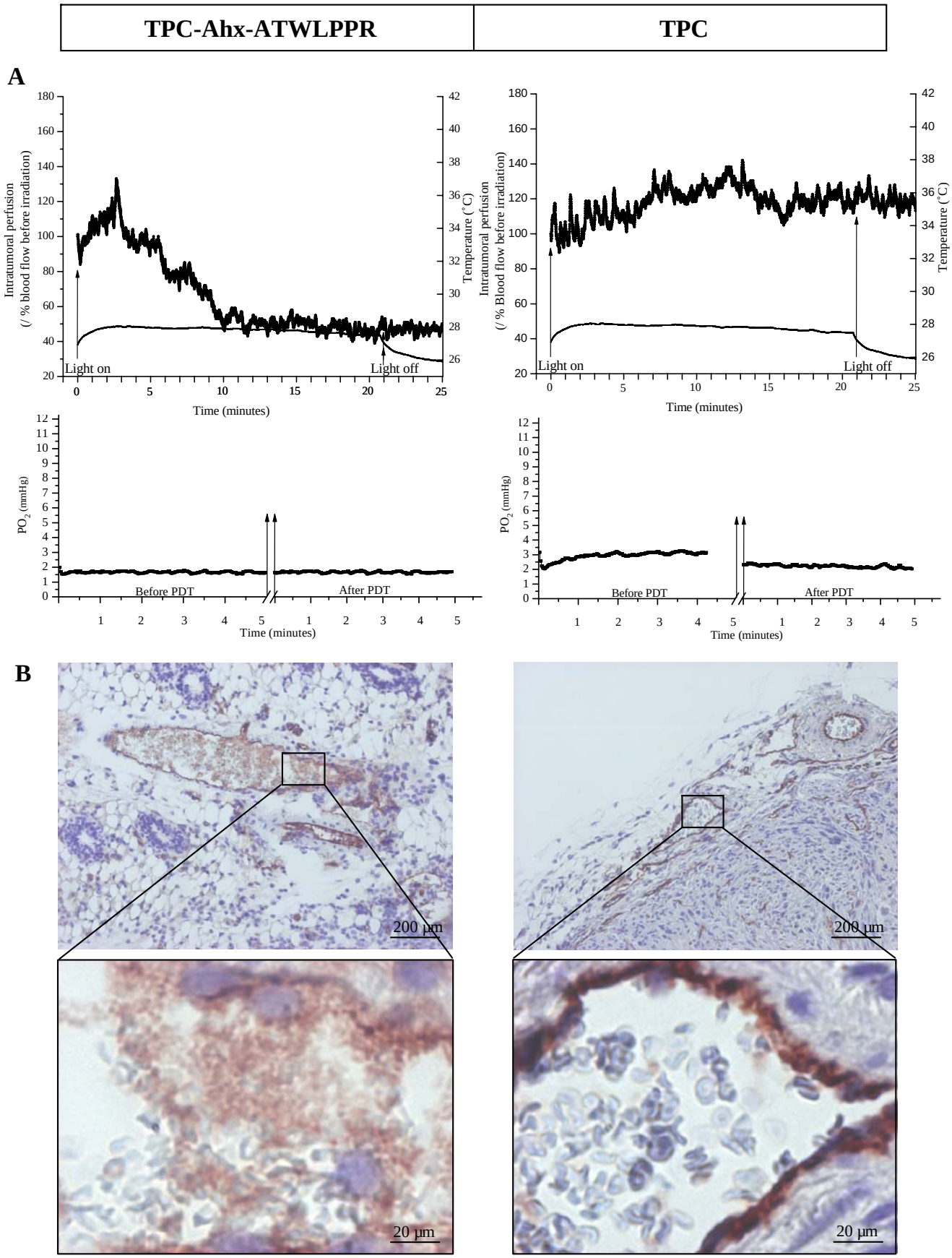
TPC-Ahx-ATWLPPR
TPC
A
Intratumoral perfusion (/ % blood flow before irradiation)
Temperature (°C)
Light on
Light off
Time (minutes)
PO2 (mmHg)
Before PDT
After PDT
B
200 µm
20 µm

◀ **Fig. 2.** Vascular-targeted PDT with TPC-Ahx-ATWLPPR induces a decrease in tumor tissue blood flow during PDT without significant variation in temperature measurements. No difference in tumor PO_2 was monitored prior to PDT compared to after treatment with optimal conditions. **A** *Upper panel*: averaged data of blood flow and traces of intratumoral temperature obtained with the laser Doppler flowmetry technique using PDT-treated tumors with TPC-Ahx-ATWLPPR (*left*) or TPC (*right*). *Lower panel:* tumor oxygenation in PDT-treated tumors. *Vertical lines* indicate the beginning of PDT (*light on*) and the end of treatment (*light off*), respectively. Results are representative of three independent experiments. **B** Histological images of the tumor capsule immediately after treatment showing red blood cells and platelets aggregation only for TPC-Ahx-ATWLPPR-mediated PDT compared to TPC. *Top*, histologic sections of the tumor tissue stained with the CD31 antibody; *bottom*, enlarged view of the corresponding specimen showing platelets aggregation with the conjugate.

the use of "vascular-targeting" agents that aim to destroy the neovasculature already formed, and which have to be distinguished from anti-angiogenic agents acting on the angiogenic process itself (30–32). Ichikawa *et al*. modified a PEG-coated liposomal BPD-MA, with the APRPG-pentapeptide binding to tumor angiogenic sites (3). Although increased uptake of photosensitizer by tumor tissue was solely attributable to the PEG moiety, conjugation to APRPG appeared necessary to suppress tumor growth efficiently.

For the first time, we propose to characterize the vascular effect of PDT using a peptide-conjugated photosensitizer targeting NRP-1 (19). As a DLI of 4 h, corresponded to the highest incorporation of TPC-Ahx-ATWLPPR in endothelial cells lining the vessels, has been chosen (17), and since our molecular marker is mainly over expressed by angiogenic vascular endothelial cells (33), the supposed initiating event would be a morphological and functional alteration of endothelium.

Blood-flow stasis is a consequence of PDT of solid tumors using many photosensitizers. TPC-Ahx-ATWLPPR-mediated VTP produced a vascular effect during treatment, including, as in many instances, an initial treatment-induced increase in tumor blood flow followed by a reduction in blood flow. A transient increase in blood flow upon illumination may be a physiological response created by photochemical oxygen consumption (34). A generalized hypothesis for the mechanisms leading to vessel stasis begins with perturbation and damage to endothelial cells during light treatment of photosensitized tissues. Using our vascular targeting strategy, measurements of blood flow stasis after VTP can arise from a combination of functional damage to endothelial cells and the resulting a physiological response to this damage. Treatment with the conjugate can alter the thrombogenic state of endothelial cells by influencing major thrombogenic pathways, thereby increasing the thrombogenic potential of the environment. Indeed, direct stimulation of endothelial cells led to the establishment of thrombogenic sites within the vessel *lumen*, and this initiated a physiological cascade of responses, including red blood cell agglutination and platelet aggregation. The formation of blood stasis and platelet

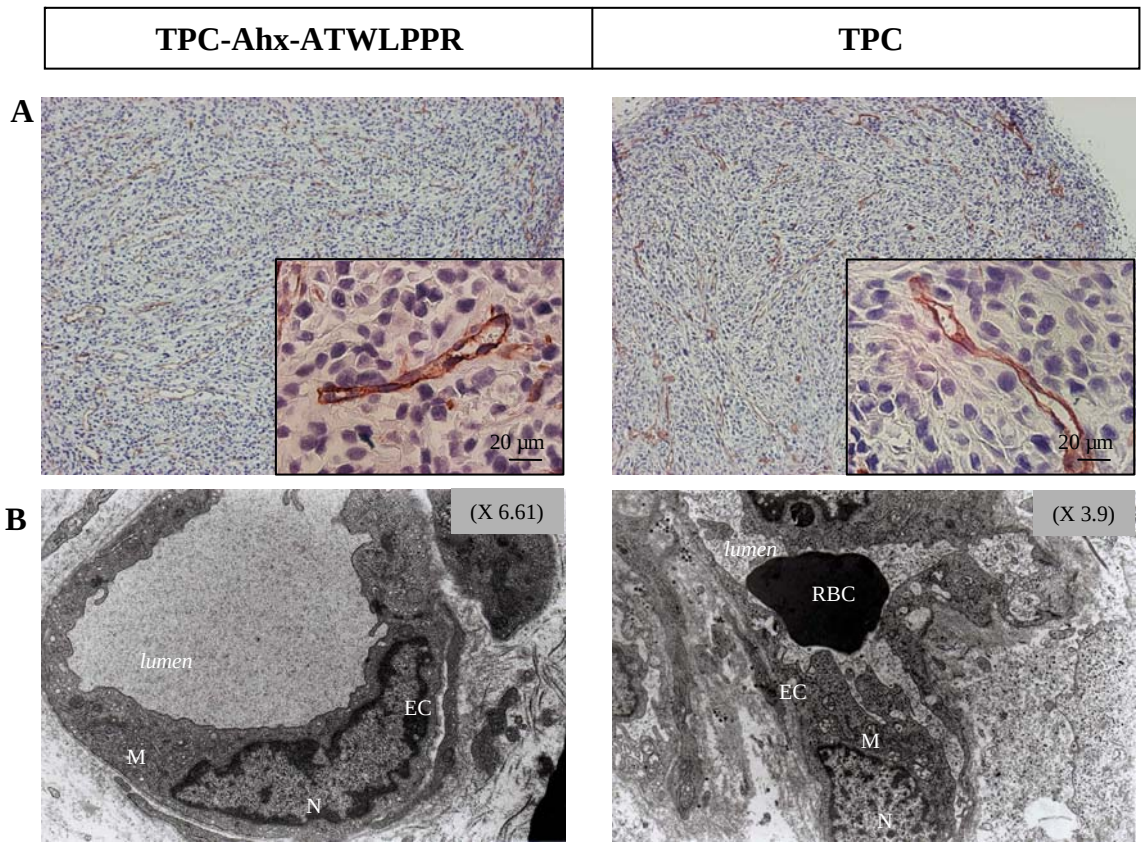

Fig. 3. Representative vessel images of CD31 staining counterstained with hematoxylin (**A**) and transmission electron microscopy (TEM) (**B**) obtained from tumor sections of the U87 tumors, immediately after treatment with optimal conditions, using either TPC-Ahx-ATWLPPR or TPC. *EC* endothelial cells; *M* mitochondria; *N* nucleus; *RBC* red blood cells.

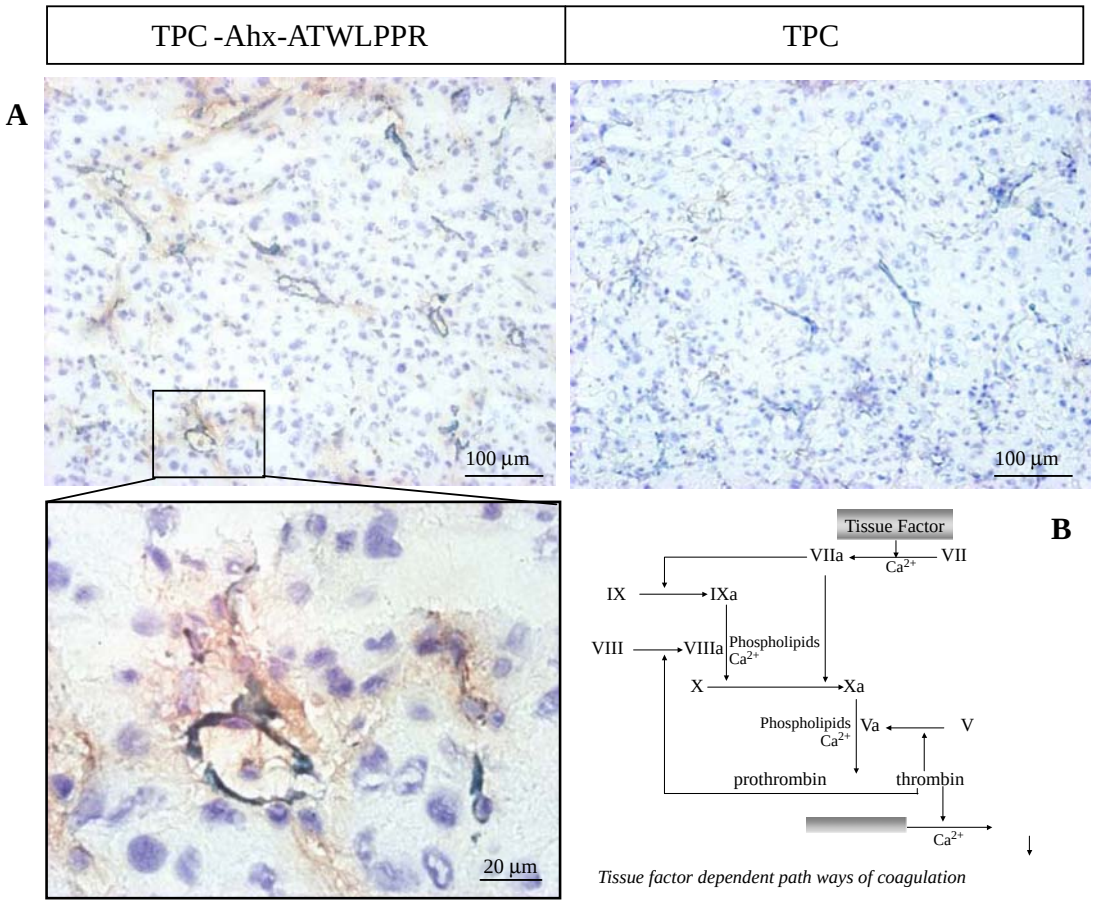

Tissue factor dependent path ways of coagulation

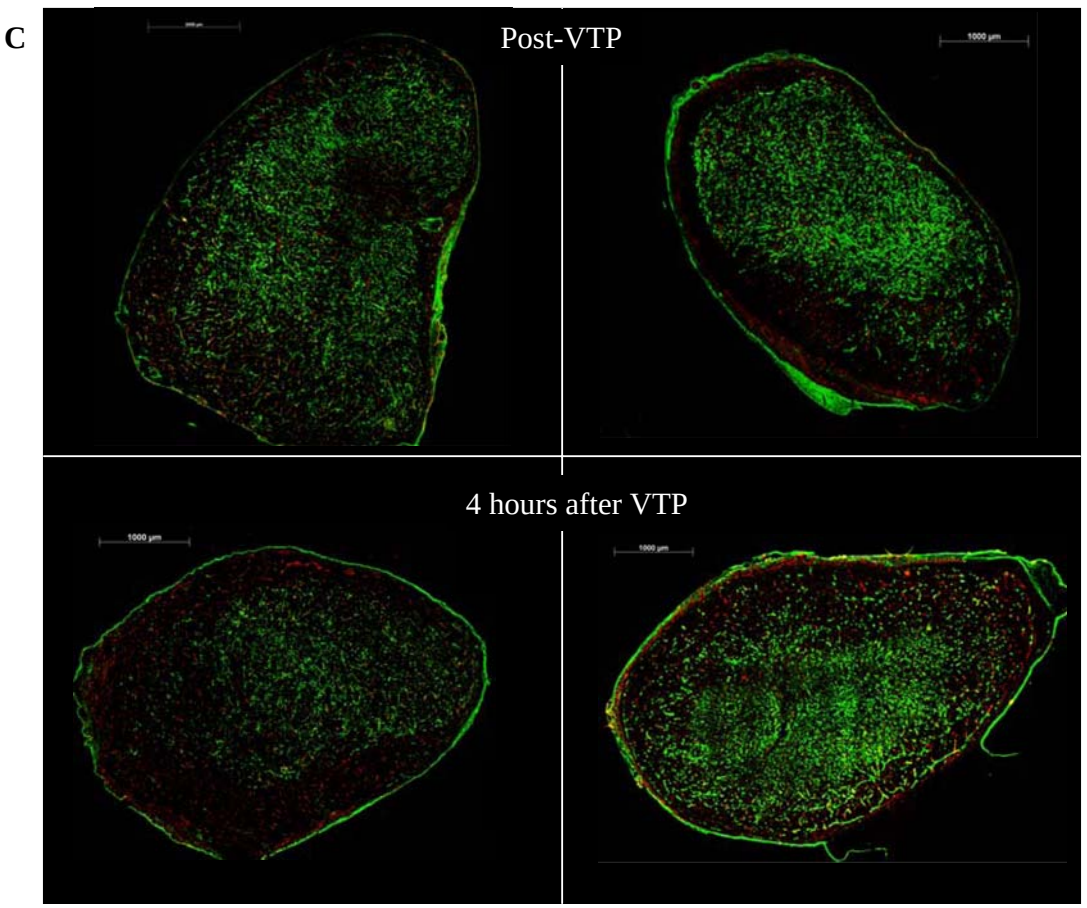

◀ **Fig. 4.** **A** immediately after treatment, TPC-Ahx-ATWLPPR-induced photodynamic activity induced TF expression (*brown staining*) compared to the non-conjugated photosensitizer. Tissue factor staining appeared to be non-uniform and was not limited to vessel *lumen* areas but also present in tumor tissues. *Bottom*, enlarged view of the corresponding specimen. **B** an illustration of the intrinsic and extrinsic pathways of blood coagulation. **C** fibrinogen consumption following TPC-Ahx-ATWLPPR-mediated PDT. Intra-tumoral patterns of fibrinogen and type IV collagen expression. Color composite images of collagen-staining [in *red*] and of fibrinogen-staining [in *green*] corresponding to the same tumor section. The relative levels of fibrinogen expression were normalized to those of collagen in order to compare the intensity of staining between TPC and the conjugate. Four hours after PDT, a decrease in the relative fibrinogen staining 0.71 *versus* 1.95 was observed for TPC-Ahx-ATWLPPR and TPC, respectively. Analysis of the tumor sections after TPC-Ahx-ATWLPPR-induced PDT showed that fibrinogen expression was mainly colocalized inside the vessels compared to its non-conjugated counterpart (Pearson correlation coefficient values 0.39 *versus* 0.08, respectively).

thrombi, leading to vessel occlusion and blood-flow alteration after PDT, has been described in several studies of rabbit eye microvasculature and ocular tumors with, for instance, BPD-MA (35,36). Functional endothelial cell damage led to the induction of the protein expression of TF. Under normal physiological conditions the vascular endothelium is a non-thrombogenic surface; endothelial cells express several anticoagulative factors (37), such as ecto-adenosine diphosphatase, heparin-like molecules and the membrane glycoprotein thrombomodulin. But after damage, they can express factors initiating the clotting cascade, the most important one being TF. Fungaloi *et al.* examined the effects of PDT on the changes in activity of thrombomodulin and TF. PDT can alter the thrombogenic state of endothelial cells decreasing thrombomodulin expression and increasing expression of functional TF in a light-energy dose-dependent way (38). In our experiments, VTP induced an increase in TF expression from endothelial cells which were capable of expressing TF after stimulation only when the tumor was treated with TPC-Ahx-ATWLPPR. It is possible that TF from endothelial cells was shed into circulation, thereby contributing to systemic thrombogenicity, suggesting that its release and diffusion may contribute to *thrombus* formation. TF can be released from cell surfaces by shedding of TF-exposing microparticles from endothelial cells (39), initiating the coagulation cascade by binding to and subsequently activating factor VII. Platelets can also internalize TF but do not generate TF (40). Cells undergoing apoptosis may become pro-coagulant by increasing TF release (41). Thus, the specific photosensitization induced by TPC-Ahx-ATWLPPR produced mainly functional

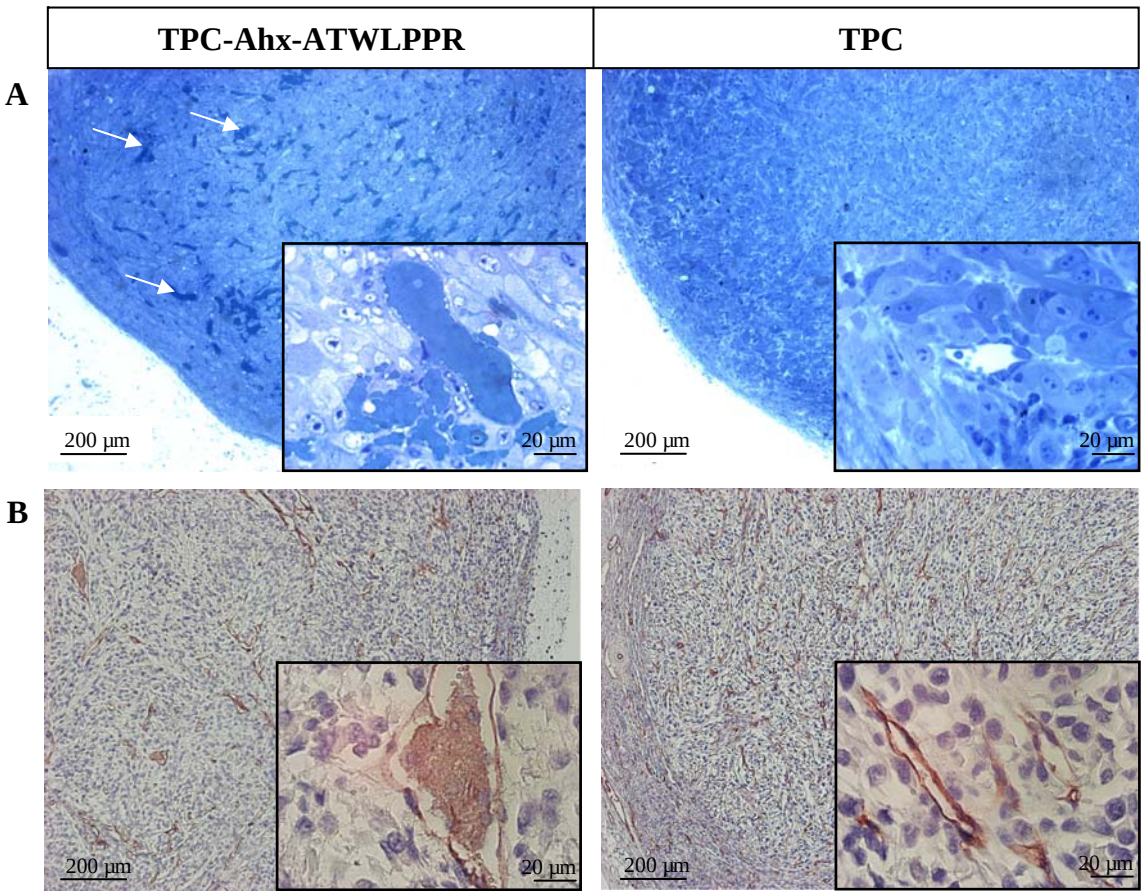

Fig. 5. Thrombogenic effect after TPC-Ahx-ATWLPPR-induced VTP. **A** 2 h post-treatment: extensive blood-vessel congestion (intense blue zones indicated by *white arrows*) were observed in tumor vasculature exclusively for mice treated with TPC-Ahx-ATWLPPR. Semithin-sections (2 µm) were stained with *toluidine blue*. *Bottom*, enlarged view of the corresponding specimen. **B** 4 h post-treatment: *thrombi* formation using TPC-Ahx-ATWLPPR compared to its non-conjugated counterpart. Representative images of CD31 staining counterstained with hematoxylin obtained from tumor sections. *Bottom*, enlarged view of the corresponding specimen.

changes of endothelial cells. Lack of fibrinogen diffusion in tumor tissue after TPC-Ahx-ATWLPPR-induced VTP suggested that photosensitization did not modify vascular permeability. This is likely because endothelial barrier function was maintained by the integrity of endothelial network at least until 4 h post-PDT. In contrast, in another study, photosensitization with verteporfin increased overall vascular permeability in both rat prostate tumor models and endothelial cells *in vitro*. According to the authors, this vascular barrier dysfunction was observed shortly after PDT, suggesting a loss of endothelial integrity (4).

Two and 4 h post-treatment, we observed for TPC-Ahx-ATWLPPR *lumen* thrombosis related to a decrease of fibrinogen expression. No massive extravasation of fibrinogen from the blood compartment into extravascular areas was evidenced. Lack of fibrinogen extravasation using this targeting strategy could be an example of inhibited extravasation of other plasma-derived proteins that may serve as an ideal matrix for endothelial cells, such as von Willebrand factor and vitronectin (42). It is well-known that fibrinogen is one of the proteins that can function as an ideal matrix for endothelial cell migration (43). Several studies have shown that fibrinogen is a component of the tumor microenvironment (44). In addition to fibrinogen, other plasma proteins are likely to serve as ideal matrix proteins for endothelial cells. A tumor vascular permeability increase may contribute to the metastatic process because sublethal PDT itself together with some tumor secreting factors (*e.g.* VEGF) could increase vascular leakiness. Moreover, localized oedema was observed at day 2 for the group treated with the conjugate. This inflammatory reaction may be secondary to the ischemic-related cell death and the cytokine production. Indeed, tumors obtained from mice treated with the conjugated photosensitizer showed the greatest increase in TNF-α and IL-6 protein levels compared to animals who received PDT with TPC. PDT-induced inflammatory changes were widely characterized by enhanced expression of a number of proinflammatory cytokines, including IL-1β, TNF-α and IL-6 (45,46). Moreover, TF pathway can also influence inflammatory signaling by activation of protease-activated receptor-1 and -2 or expression of TNF-α and IL-6 (47). Szotowski *et al.* explained that the asHTF (alternatively spliced human tissue factor) released from endothelial cells contributes to create an imbalance in homeostasis. This soluble TF isoform released from endothelial cells in response to inflammatory cytokines becomes procoagulant in presence of phospholipids (47). The inductive phase of inflammation, mounted during PDT light treatment or immediately thereafter, could be associated with a prompt release of pro-inflammatory mediators and rapid expression of genes encoding inflammatory chemoattractants, cytokines, leukocyte adhesion molecules, degradative enzymes, and other mediators (48). Some of these mediators (*e.g.*, cytokines) can also be released from cells sustaining injury by direct PDT damage (45,49).

Treatment of glioma-bearing mice with the peptide-conjugated TPC showed a statistically significant reduction in tumor growth compared with animals who received PDT with TPC. This strategy of targeting NRP-1 improves the potential of VTP. Nevertheless, treatment with TPC-Ahx-ATWLPPR led to a halt in tumor growth rather than regression, even if we observed tumor-free mice (30%, 40 days post-treatment). It is not excluded that pro-angiogenic factors secreted could also induce compensatory changes in the existing vasculature toward more mature blood vessels. This vasculature phenotype ensures maintenance of the established tumor mass and may be resistant to our targeting strategy. Our future efforts will focus on exploring the therapeutic potential of fractionated VTP.

ACKNOWLEDGEMENTS

The authors would like to thank Denise Thiébaut, Marie Rouyer, and Carole Ramacci for their excellent technical assistance. We also thank Sophie Pinel and Anne-Sophie Chrétien for their collaboration. This work was supported by the research funds of the French "Ligue Nationale Contre le Cancer, Comités Lorrains."

REFERENCES

1. Folkman J. Angiogenesis in cancer, vascular, rheumatoid and other disease. Nat Med. 1995;1:27–31.
2. Dougherty TJ, Gomer CJ, Henderson BW, Jori G, Kessel D, Korbelik M, *et al.* Photodynamic therapy. J Natl Cancer Inst. 1998;90:889–905.
3. Ichikawa K, Hikita T, Maeda N, Yonezawa S, Takeuchi Y, Asai T, *et al.* Antiangiogenic photodynamic therapy (PDT) by using long-circulating liposomes modified with peptide specific to angiogenic vessels. Biochim Biophys Acta. 2005;1669:69–74.
4. Chen B, Pogue BW, Luna JM, Hardman RL, Hoopes PJ, Hasan T. Tumor vascular permeabilization by vascular-targeting photosensitization: effects, mechanism, and therapeutic implications. Clin Cancer Res. 2006;12:917–23.
5. Fingar VH, Taber SW, Haydon PS, Harrison LT, Kempf SJ, Wieman TJ. Vascular damage after photodynamic therapy of solid tumors: a view and comparison of effect in pre-clinical and clinical models at the University of Louisville. In Vivo. 2000;14:93–100.
6. Huang Z, Chen Q, Luck D, Beckers J, Wilson BC, Trncic N, *et al.* Studies of a vascular-acting photosensitizer, Pd-bacteriopheophorbide (Tookad), in normal canine prostate and spontaneous canine prostate cancer. Lasers Surg Med. 2005;36:390–7.
7. McMahon KS, Wieman TJ, Moore PH, Fingar VH. Effects of photodynamic therapy using mono-L-aspartyl chlorin e6 on vessel constriction, vessel leakage, and tumor response. Cancer Res. 1994;54:5374–9.
8. Wieman TJ, Mang TS, Fingar VH, Hill TG, Reed MW, Corey TS, *et al.* Effect of photodynamic therapy on blood flow in normal and tumor vessels. Surgery. 1988;104:512–7.
9. Fingar VH, Wieman TJ, Wiehle SA, Cerrito PB. The role of microvascular damage in photodynamic therapy: the effect of treatment on vessel constriction, permeability, and leukocyte adhesion. Cancer Res. 1992;52:4914–21.
10. Fingar VH. Vascular effects of photodynamic therapy. J Clin Laser Med Surg. 1996;14:323–8.
11. Henderson BW, Dougherty TJ. How does photodynamic therapy work? Photochem Photobiol. 1992;55:145–57.
12. Kurohane K, Tominaga A, Sato K, North JR, Namba Y, Oku N. Photodynamic therapy targeted to tumor-induced angiogenic vessels. Cancer Lett. 2001;167:49–56.
13. Chen B, Pogue BW, Hoopes PJ, Hasan T. Vascular and cellular targeting for photodynamic therapy. Crit Rev Eukaryot Gene Expr. 2006;16:279–305.
14. Starzec A, Ladam P, Vassy R, Badache S, Bouchemal N, Navaza A, *et al.* Structure-function analysis of the antiangiogenic ATWLPPR peptide inhibiting VEGF(165) binding to neuropilin-1 and molecular dynamics simulations of the ATWLPPR/neuropilin-1 complex. Peptides. 2007;28:2397–402.
15. Tirand L, Frochot C, Vanderesse R, Thomas N, Trinquet E, Pinel S, *et al.* A peptide competing with VEGF165 binding on

neuropilin-1 mediates targeting of a chlorin-type photosensitizer and potentiates its photodynamic activity in human endothelial cells. J Control Release. 2006;111:153–64.
16. Thomas N, Bechet D, Becuwe P, Tirand L, Vanderesse R, Frochot C, *et al*. Peptide-conjugated chlorin-type photosensitizer binds neuropilin-1 *in vitro* and *in vivo*. J Photochem Photobiol B. 2009;96:101–8.
17. Thomas N, Tirand L, Chatelut E, Plenat F, Frochot C, Dodeller M, *et al*. Tissue distribution and pharmacokinetics of an ATWLPPR-conjugated chlorin-type photosensitizer targeting neuropilin-1 in glioma-bearing nude mice. Photochem Photobiol Sci. 2008;7:433–41.
18. Tirand L, Bastogne T, Bechet D, Linder M, Thomas N, Frochot C, *et al*. Response surface methodology: an extensive potential to optimize *in vivo* photodynamic therapy conditions. Int J Radiat Oncol Biol Phys. 2009;75:244–52.
19. Tirand L, Thomas N, Dodeller M, Dumas D, Frochot C, Maunit B, *et al*. Metabolic profile of a peptide-conjugated chlorin-type photosensitizer targeting neuropilin-1: an *in vivo* and *in vitro* study. Drug Metab Dispos. 2007;35:806–13.
20. Pinel S, Barberi-Heyob M, Cohen-Jonathan E, Merlin JL, Delmas C, Plenat F, *et al*. Erythropoietin-induced reduction of hypoxia before and during fractionated irradiation contributes to improvement of radioresponse in human glioma xenografts. Int J Radiat Oncol Biol Phys. 2004;59:250–9.
21. Chergui F, Chretien AS, Bouali S, Ramacci C, Rouyer M, Bastogne T, *et al*. Validation of a phosphoprotein array assay for characterization of human tyrosine kinase receptor downstream signaling in breast cancer. Clin Chem. 2009;55:1327–36.
22. Yu G, Durduran T, Zhou C, Wang HW, Putt ME, Saunders HM, *et al*. Noninvasive monitoring of murine tumor blood flow during and after photodynamic therapy provides early assessment of therapeutic efficacy. Clin Cancer Res. 2005;11:3543–52.
23. Kelleher DK, Thews O, Scherz A, Salomon Y, Vaupel P. Perfusion, oxygenation status and growth of experimental tumors upon photodynamic therapy with Pd-bacteriopheophorbide. Int J Oncol. 2004;24:1505–11.
24. Dudar TE, Jain RK. Differential response of normal and tumor microcirculation to hyperthermia. Cancer Res. 1984;44:605–12.
25. Mackman N. Regulation of the tissue factor gene. Faseb J. 1995;9:883–9.
26. Archipoff G, Beretz A, Freyssinet JM, Klein-Soyer C, Brisson C, Cazenave JP. Heterogeneous regulation of constitutive thrombomodulin or inducible tissue-factor activities on the surface of human saphenous-vein endothelial cells in culture following stimulation by interleukin-1, tumour necrosis factor, thrombin or phorbol ester. Biochem J. 1991;273(Pt 3):679–84.
27. Siemann DW, Chaplin DJ, Horsman MR. Vascular-targeting therapies for treatment of malignant disease. Cancer. 2004;100: 2491–9.
28. Brekken RA, Li C, Kumar S. Strategies for vascular targeting in tumors. Int J Cancer. 2002;100:123–30.
29. Dolmans DE, Kadambi A, Hill JS, Waters CA, Robinson BC, Walker JP, *et al*. Vascular accumulation of a novel photosensitizer, MV6401, causes selective thrombosis in tumor vessels after photodynamic therapy. Cancer Res. 2002;62:2151–6.
30. Eichhorn ME, Strieth S, Dellian M. Anti-vascular tumor therapy: recent advances, pitfalls and clinical perspectives. Drug Resist Updat. 2004;7:125–38.
31. Thorpe PE, Chaplin DJ, Blakey DC. The first international conference on vascular targeting: meeting overview. Cancer Res. 2003;63:1144–7.
32. Ebos JM, Lee CR, Cruz-Munoz W, Bjarnason GA, Christensen JG, Kerbel RS. Accelerated metastasis after short-term treatment with a potent inhibitor of tumor angiogenesis. Cancer Cell. 2009;15:232–9.
33. Klagsbrun M, Takashima S, Mamluk R. The role of neuropilin in vascular and tumor biology. Adv Exp Med Biol. 2002;515:33–48.
34. Leach RM, Hill HS, Snetkov VA, Ward JP. Hypoxia, energy state and pulmonary vasomotor tone. Respir Physiol Neurobiol. 2002;132:55–67.
35. Lin SC, Lin CP, Feld JR, Duker JS, Puliafito CA. The photodynamic occlusion of choroidal vessels using benzoporphyrin derivative. Curr Eye Res. 1994;13:513–22.
36. Fingar VH, Kik PK, Haydon PS, Cerrito PB, Tseng M, Abang E, *et al*. Analysis of acute vascular damage after photodynamic therapy using benzoporphyrin derivative (BPD). Br J Cancer. 1999;79:1702–8.
37. Wu KK, Thiagarajan P. Role of endothelium in thrombosis and hemostasis. Annu Rev Med. 1996;47:315–31.
38. Fungaloi P, Waterman P, Nigri G, Statius-van Eps R, Sluiter W, van Urk H, *et al*. Photochemically modulated endothelial cell thrombogenicity via the thrombomodulin-tissue factor pathways. Photochem Photobiol. 2003;78:475–80.
39. Wada H, Wakita Y, Shiku H. Tissue factor expression in endothelial cells in health and disease. Blood Coagul Fibrinolysis. 1995;6 Suppl 1:S26–31.
40. Zillmann A, Luther T, Muller I, Kotzsch M, Spannagl M, Kauke T, *et al*. Platelet-associated tissue factor contributes to the collagen-triggered activation of blood coagulation. Biochem Biophys Res Commun. 2001;281:603–9.
41. Bombeli T, Karsan A, Tait JF, Harlan JM. Apoptotic vascular endothelial cells become procoagulant. Blood. 1997;89:2429–42.
42. Fungaloi P, Statius van Eps R, Wu YP, Blankensteijn J, de Groot P, van Urk H, *et al*. Platelet adhesion to photodynamic therapy-treated extracellular matrix proteins. Photochem Photobiol. 2002;75:412–7.
43. Liu HM, Wang DL, Liu CY. Interactions between fibrin, collagen and endothelial cells in angiogenesis. Adv Exp Med Biol. 1990;281:319–31.
44. Daly ME, Makris A, Reed M, Lewis CE. Hemostatic regulators of tumor angiogenesis: a source of antiangiogenic agents for cancer treatment? J Natl Cancer Inst. 2003;95:1660–73.
45. Evans S, Matthews W, Perry R, Fraker D, Norton J, Pass HI. Effect of photodynamic therapy on tumor necrosis factor production by murine macrophages. J Natl Cancer Inst. 1990;82:34–9.
46. Seshadri M, Bellnier DA. The vascular disrupting agent 5, 6-dimethylxanthenone-4-acetic acid improves the antitumor efficacy and shortens treatment time associated with Photochlor-sensitized photodynamic therapy *in vivo*. Photochem Photobiol. 2009;85:50–6.
47. Szotowski B, Antoniak S, Poller W, Schultheiss HP, Rauch U. Procoagulant soluble tissue factor is released from endothelial cells in response to inflammatory cytokines. Circ Res. 2005;96:1233–9.
48. Korbelik M, Cecic I. Mechanism of tumor destruction by photodynamic therapy. In: Nalwa HS, editor. Handbook of photocochemistry and photobiology, vol. 4. Stevenson Ranch: American Scientific Publishers; 2003. p. 39–77.
49. Karrer S, Bosserhoff AK, Weiderer P, Landthaler M, Szeimies RM. Keratinocyte-derived cytokines after photodynamic therapy and their paracrine induction of matrix metalloproteinases in fibroblasts. Br J Dermatol. 2004;151:776–83.